Text: 1,694 words (excluding summary, methods, references and legends)
Text: 4,133 (excluding references)
References: 35
4 main figures (approximate final size of figures: 10x13 cm)
9 supplementary figures
Expected number of Nature pages: 5

The tumour suppressor Pml regulates cell fate in the developing neocortex

Tarik Regad, Cristian Bellodi, Pierluigi Nicotera & Paolo Salomoni*

MRC Toxicology Unit, Leicester LE1 7JL, United Kingdom

*To whom the correspondence should be addressed. E-mail: ps90@le.ac.uk

The control of cell fate in neural progenitor/stem cells is critical for nervous system development [1, 2]. Nevertheless, the players involved are only partially known. We found that in the developing neocortex the expression of the tumour suppressor Pml is restricted to neural progenitor cells (NPCs). Remarkably, in *Pml-/-* cortices the overall number of proliferating NPCs is increased, while transition between the two major progenitor types, radial glial cells and basal progenitors is impaired. This in turn results in reduced differentiation and an overall decrease in thickness of the cortex wall. In NPCs, Pml regulates the subcellular distribution of the retinoblastoma protein (pRb) and the protein phosphatase 1 α (PP1α), triggering pRb dephosphorylation. Together, these findings reveal an unexpected role of Pml in controlling the function of NPCs in the central nervous system.

The gene encoding the promyelocytic leukaemia protein (PML) is a tumour suppressor originally identified at the breakpoint of the t(15;17) translocation found in acute promyelocytic leukaemia (APL) ([3, 4] and references cited therein). Pml is associated with a subnuclear structure known as the PML-nuclear domain (PML-ND), of which it is the essential component [5-7]. Pml is a potent growth suppressor in both cell lines and primary cells and regulates the tumour suppressors p53 and pRb [4, 8-10]. Recent studies suggest that Pml exerts its tumour suppressive function also outside the haemopoietic system [4, 11-13]. In particular, Pml expression is lost in human tumours of multiple histological origins including tumours of the central nervous system, such as medulloblastoma[4, 11].

Correct regulation of cell cycle progression has been shown to be essential during the development of the nervous system (reviewed in [1, 2, 14]). In particular, the neural epithelium lying in the apical area of the developing neocortex gives rise to progenitors, post-mitotic neurons and macroglia in a temporally and spatially controlled fashion (reviewed in [1, 2]). How the balance between proliferation and differentiation of neural progenitors is maintained during early development and which are the main players involved remain central questions in the field of neurodevelopment [14, 15].

The role of Pml in the development of the nervous system is completely unexplored. We found that in the developing cerebral cortex Pml expression is

confined to the neuroepithelial zone, where Nestin-positive neural stem / progenitor cells lie (Fig. 1a) [16]. By contrast, Pml was not detected in the cortical plate of *Pml-/-* cortices and in early-born βIII Tubulin (βIIITub)-positive neurons in the ventricular zone (Fig. 1a and 1b). At the subcellular level, Pml accumulated in nuclear speckles (Fig. 1a). Pml expression was restricted to the progenitors zone also at postnatal day 0 (P0) and at P7 (Supplementary Fig. 1a, b). Cortical precursors divide to give rise to different types of differentiated cells that in turn migrate radially to specific layers in the cortical plate (reviewed in [1]). To test whether Pml plays a role in neocortex development, we analysed brains isolated from *Pml+/+*, *Pml+/-* and *Pml-/-* animals at P0 (total n=32), when neuronal differentiation is complete. Analysis of haematoxylin and eosin (H&E)-stained coronal sections clearly showed that, while the overall organisation of the brain does not appear to be affected in *Pml-/-* mice, the cerebral cortex appears smaller (Fig. 1c). This effect was not solely restricted to the cortex, as also the size of the hippocampus appeared to be affected at P0 (Suppl. Fig. 2). Moreover, the width and length of cortex in whole brains was reduced (Fig. 1d) and the overall thickness of the cortex wall was also diminished (Fig. 1e). Finally, Pml-/- adult brains show more modest albeit significant differences in thickness of the cortical wall, thus suggesting a degree of compensation at later stages (Suppl Fig. 3a, b). Taken together, these findings demonstrate that Pml loss affects the size of the cerebral cortex.

As mentioned above, the development of the neocortex relies on correct cell cycle regulation at the level of neural progenitor/stem cells in the VZ [1, 2]. Therefore, as Pml is a growth suppressor, we reasoned that its loss could affect cell cycle in neural progenitors. We analysed the number of proliferating cells in the E15 VZ by using the Ki67 and PCNA proliferation markers and found that *Pml-/-* cortices presented an expanded pool of cycling cells (Fig. 2a and not shown). We also detected an increased number of mitotic cells at the apical side of the VZ using the mitotic marker phospho-histone H3 (Fig. 2b). In order to determine the number of cells in the S-phase of cell cycle, we injected 15-days pregnant females intraperitoneally (i.p.) with bromodeoxyuridine (BrdU). After a one-hour pulse, BrdU-labelled control cells were located basally in the VZ due to intrakinetic nuclear migration (Fig. 2c) [1, 2]. The number of cells in S phase was clearly elevated in the *Pml-/-* cortex, while nuclear positioning did not appear to be substantially affected

(Fig. 2c). A similar increase in the number of Ki67-positive progenitors was observed in *Pml-/-* animals at P0 and P7 (Suppl. Fig. 4). Differences in proliferation of progenitors were also demonstrated *in vitro* using the neurosphere assay [19]. For instance, the diameter of neurospheres from *Pml-/-* E12 embryos was approximately twice the one of controls after 10 days *in vitro* (DIV10) at clonal density (Fig. 2d), and their number was also increased (not shown). Notably, Pml loss appeared to affect the transition between the two major types of progenitors present in the VZ, radial glial and basal progenitors [17, 18], as an increased number of Pax6-positive radial glial cells was accompanied by a reduction in basally-located progenitors, which were identified using the Tbr2 and P-H3 markers (Fig. 2e, f, g) [17, 18]. Finally, developmental cell death was normal in mutant cortices at E15 (Suppl. Fig. 5), thus suggesting that the higher number of progenitors found in *Pml-/-* brains is caused by increased proliferation.

Two cell cycle parameters are believed to regulate the development of the neocortex: cell cycle exit and cell cycle re-entry [14]. We set out to investigate whether cell cycle exit is affected in Pml-deficient progenitors *in vivo*. To this end, we determined the number of BrdU+ and Ki67+ cells after a 24 hours BrdU pulse at E15 (n=3 *Pml-/-* and n=3 *Pml+/-* littermates). In this assay, BrdU+ / Ki67+ cells represent cells in cycle while, BrdU+ / Ki67- are cells that exited cell cycle. We found a two-fold decrease in the number of cells exiting the cell cycle in *Pml-/-* cortices (Fig. 2h). Furthermore, the number of Ki67+/BrdU- cells present in the KO VZ was diminished, suggesting that a larger portion of proliferating cells enter S-phase compared to controls. This probably reflects shortening of the cell cycle. Taken together, these findings suggest that a greater proportion of *Pml-/-* progenitors re-enter cell cycle after mitosis and that Pml loss may alter the balance between cell cycle exit and re-entry. Based on the models currently available [14], decreased cell cycle exit would affect generation of neurons. Indeed, we revealed a significant decrease in the number of MAP2-positive neuronal cells at E15 (Fig. 3a, Suppl. Fig. 6a) and P0 (Fig. 3b, Supplementary Fig. 6b) in the *Pml-/-* cortical plate. However, the layered structure of the cortex and neuronal specification did not appear to be affected in *Pml-/-* animals, as deep layer 6 (Foxp2+) and layers 3-4-5 (Foxp1+), despite containing a reduced number of cells, were correctly positioned (Suppl. Fig. 7). Generation of astrocytes (GFAP+) and oligodendrocytes (MBP+) was also affected in the *Pml-/-* cerebral

cortex at P7 (Suppl. Fig. 6c). *In vitro* differentiation assays demonstrated that Pml loss results in an overall reduction of MAP2+ neurons, accompanied by an increase in Nestin+ cells (DIV5; Fig. 3c, Suppl. Fig. 8). Also differentiation into astrocytes and oligodendrocytes was affected in *Pml-/-* cultures (DIV10; Fig. 3c, Suppl. Fig. 8). Reintroduction of PML I in *Pml-/-* progenitors results in decreased size of neurospheres and rescued differentiation (Fig. 3d, e). Interestingly, mutation of the PML SUMOylation sites governing PML-ND formation (ΔSUMO-PML I) [7] abolished the effect on proliferation and differentiation in Pml-deficient cells (Fig. 3d, e), thus suggesting that formation of PML-ND is a prerequisite for PML I activity in cortical progenitors.

Among Pml interactors, the Retinoblastoma protein (pRb) [9, 20-22] has an established role in nervous system development and pathogenesis of brain tumours [23-28]. However, pRb function at the level of neural precursors is still unclear. We found that in cortical progenitors pRb accumulates in nuclear speckles, which partially colocalize with PML-NDs (Fig. 4a). In contrast, in *Pml-/-* cells pRb was more nucleoplasmic and also accumulated in the cytoplasm (Fig. 4a). Similar staining pattern was obtained using a different anti-pRb antibody (Suppl. Fig. 9a). These changes did not occur in the cortical plate, where Pml is not normally expressed, thus confirming the specificity of the observed alterations (Fig. 4a; Suppl. Fig. 9a, c). Furthermore, we found that pRb and Pml interact in neural progenitors (Fig. 4b). pRb is inactivated through phosphorylation by cyclin-dependent kinases [29]. Interestingly, in *Pml-/-* cortical progenitors cells pRb was hyperphosphorylated, thus suggesting that Pml regulates pRb phosphorylation status (Fig. 4c), as proposed by previous studies [9, 22]. Cyclin-dependent phosphorylation of pRb is counteracted by the activity of the protein phosphatase 1α (PP1α) [30, 31], which has been recently implicated in neocortex development [32]. We found that Pml, pRb and PP1α colocalize in the nucleus of neuronal progenitors both *in vivo* and *in vitro* (Fig. 4d, e; Suppl. Fig. 9b, c). Instead, in *Pml-/-* cortices and isolated cortical progenitors PP1α localization changed to a more diffuse nuclear staining and cytoplasmic accumulation (Fig. 4d, e and Suppl. Fig. 9b, c). Finally, both pRb and PP1α are found in anti-Pml immunoprecipitates, thus suggesting that the three proteins form a nuclear complex (Fig. 4f). Reintroduction of PML I isoform in *Pml-/-* progenitors resulted in decreased pRb phosphorylation (Fig. 4g). In contrast, the ΔSUMO-PML I mutant failed to affect pRb

phosphorylation (Fig. 4g). Finally, the effect on phosphorylation was completely abolished in the presence of the PP1α inhibitor tautomycetin (not shown).

Overall, our results provide evidence of a novel Pml role in regulating cell fate in neural progenitor/stem cells. In particular, Pml loss appears to affect proliferation of radial glial cells and to inhibit the transition to basal progenitors. This in turn leads to impaired differentiation and reduced size of the cortex. As for the underlying mechanism, we propose a model by which Pml controls cell cycle in neural progenitor/stem cells by affecting pRb phosporylation status, thus potentially revealing a novel role of pRb outside the pool of maturing neurons [24, 25, 28, 33]. More generally, our work shows that an increased number of progenitors in the developing cerebral cortex does not necessarily result in augmented neurogenesis, but instead it can lead to a block of differentiation and in turn to a decrease in cortex size. Finally, our findings, together with the reported loss of PML expression in human brain tumours [11], opens up the possibility that alterations of PML function may be involved in the onset of neoplastic disorders originating from the neuroepithelial compartment of the nervous system.

METHODS

Animals

Pml-/- animals were a generous gift from Dr. Pier Paolo Pandolfi (Harvard University, Boston, USA). Animals were backcrossed to the sv129 S2 strain for eight generations. Animals were bred and subjected to listed procedures under the Project Licence no. 80-2085, released from the Home Office.

Antibodies

Anti-PML (05-718; 1/500 for IB, 1/100 for IHC, IF and IP) from Upstate/Millipore; Anti-BrdU-fluorescin from Roche (1202693; 1/1000), anti-MAP2 (ab11267; 1/50), anti-FOXP1 (ab16645; 1/200), anti-FOXP2 (ab16046; 1/2500) and anti-Rb (ab6075; 1/50 for IHC and IF) from Abcam; anti-MBP (AB980; 1/500), anti-PML (AB1370) and anti-Nestin (MAB353; 1/500) from Chemicon; anti–pRb (554136; 1/100 for IB) from BD Pharmingen; anti-β-actin from Sigma (A2172; 1/5000); anti GFAP (Z0334; 1/500) from Dako, anti-PP1α (sc-6104; 1/100 for IHC and IF, 1/500 for IB) from Santa Cruz Biotechnology; anti-Ki67 (NCL-Ki67p; 1/500) from Novocastra; anti-Pax6 (supernatant concentrate; 1/200) from DSHB/University of Iowa; anti-Tbr2 (IHC/IF 1:2,000; a kind gift from Dr Hevner, Seattle Children's Hospital Research Institute, Seattle, USA) anti-active caspase 3 (9661S; 1/200) from Cell signalling; anti-phospho H3 (1:200) from Upstate/Millipore.

Immunohistochemistry and immunofluorescence

E12, P0 or P7 brains were fixed in 4% paraformaldehyde and embedded in paraffin. The sections were de-waxed, re-hydrated in graded alcohols, rinsed in distilled water and antigen retrieval treated for 30 minutes (0.01 M citric acid at pH 6.0) in pressure cooker at 700 Watts. For staining of isolated cells, cortical cells were prepared and treated as explained below and fixed in 4% paraformaldehyde. The sections or cortical cells were washed in PBS 1x for 3X10 minutes, blocked in 10% goat serum in 0.1% PBS-Tween followed by overnight first antibody incubation (in blocking solution), washed three times 10 minutes with PBS 1x, an 1h incubation with secondary antibody (in blocking solution) then three times wash with PBS 1x and counterstained with DAPI and mounted for confocal microscopy. For triple staining experiments, all immunofluorescence steps were performed using 5% bovine serum albumin (BSA) as blocking reagent. Two different images of each section or cortical cells were taken and the number of cells labelled was counted (n=3 PML null compared to n=3 control littermates).

BrdU labelling

Pregnant females at E15 days of gestation were injected intraperitoneally for 1hour with 50μg/g body mass bromodeoxyuridine (BrdU). One hour after, the females were culled and the embryos removed, fixed in 4% paraformaldehyde and embedded in paraffin. Sections were stained with anti-BrdU-fluorescin isothiocyanate (FITC) antibody. The number of BrdU-labeled cells was determined by counting BrdU+ cells from two confocal microscopy images of corresponding sections from 3 independent experiments (n=3 PML null compared to n=3 control littermates).

For the cell cycle exit experiment, pregnant females at E14 were injected with BrdU as described above for 24 hours, culled and the embryos removed, fixed in 4% parafolmaldehyde and embedded in paraffin for sectioning. The sections were co-

stained with anti-BrdU-fluorescin isothiocyanate and Ki67 antibodies. The cells counted in this experiment are the ones that exited the cell cycle (BrdU + only) and are localised in the Intermediate zone after radial migration. The cells that are still proliferating or remain in the cell cycle are BrdU+ and Ki67+ and are localised in the VZ.

Immunoblotting and Immnunoprecipitation

For immunoblotting, cortical neurospheres were collected, washed with 1x PBS then lysed in 1x solution containing 50mM Tris-HCl (pH 6.8), 100mM dithiothreitol, 2% SDS, 0.1 bromophenol blue and 10% glycerol prior loading on Tris/glycine SDS-polyacrylamide gels. For immunoprecipitation, the cortical cells were lysed in immunoprecipitation (IP) buffer (0.05M Tris pH 7.4, 0.15M NaCl, 0.5% Triton, 0.001M EDTA). The extracts were precleared for 1hour at 4^{o}C using Protein G Plus-Agarose beads (IP08, Calbiochem) and anti-IgG2b (Dako). For the antibody binding, anti-PML was incubated with agarose beads for 2 hours in IP buffer prior adding the precleared extracts overnight for immunoprecipitation.

Cortical cell culture

Cortical cultures were prepared using reagents from Stem Cell Technologies and following the manufacturer's protocol and previously reported protocols [19]. For the neurospheres culture, the cortical cells were plated at clonal density (20x10^3 cells/ml in 24-well plates) in complete neurocult neural stem cells (NSC) proliferation medium containing 10 ng/ml bFGF (Peprotech) and cultured for 10 days in vitro (DIV). For the differentiation assay, single cell suspensions of cortical cells were plated at 5x10^5 cells/well on poly-L-ornithine glass coverslips in complete neurocult NSC differentiation media. At DIV5 cells were fixed in 4% paraformaldehyde and analyzed for expression of the progenitor marker Nestin and the neuronal marker MAP2 by immunofluorescence. Instead, at DIV10 cells were stained with antibodies against Nestin and MBP and GFAP, which are markers for oligodendrocytes and astrocytes, respectively [34]. The PP1α inhibitor (InSolution Tautomycetin, *S. greseochrogenes*; cat no. 580550 Calbiochem) was added to the neurospheres culture (5μM) for 5.5 hours.

Retroviral expression of PML

PML isoform V cDNA (kind gift from David Grimwade) was cloned into the EcoRI site of pBabePuro (pBabe). Then, a PCR-amplified fragment containing the PML I-specific C-term was cloned into Mlu I/ Sal I sites of PML V pBabe to obtain PML I pBabe. The PML I mutant lacking PML's three SUMOylation sites (ΔSUMO PML I pBabe) was generated by site-directed mutagenesis. Cortical cells were infected with high-titer pBabe, pBabe-PML I or pBabe ΔSUMO PML I retroviral supernatants and selected in puromycin (Sigma) for 48 hours [35].

ACKNOWLEDGMENTS

A special thank to Dr Hevner (Seattle Children's Hospital Research Institute, Seattle, USA) for the anti-Tbr2 antibody, and to David Dinsdale, Jenny Edwards and Richard Edwards (MRC Toxicology Unit, Leicester, UK) for support and assistance with immunohistochemistry. We also thank Christine Watson (University of Cambridge, UK), David Read, Gerry Melino, Richard Knight, and Melania Capasso (MRC Toxicology Unit, Leicester, UK) for critical discussion. P.S., P.N., T.R., and C.B. are supported by the MRC, UK. C.B. is a PhD student at the University of Leicester.

AUTHOR CONTRIBUTION

T.R. performed most of the experiments and contributed to the writing of the manuscript; C.B. performed a number of experiments; P.N. provided expertise; P.S. supervised the research project, performed a number of experiments and wrote the manuscript.

REFERENCES

1. Campbell, K. Cortical neuron specification: it has its time and place. *Neuron* **46**, 373-6 (2005).
2. Guillemot, F. Cellular and molecular control of neurogenesis in the mammalian telencephalon. *Curr Opin Cell Biol* **17**, 639-47 (2005).
3. Melnick, A. & Licht, J. D. Deconstructing a disease: RARalpha, its fusion partners, and their roles in the pathogenesis of acute promyelocytic leukemia. *Blood* **93**, 3167-215 (1999).
4. Salomoni, P., Ferguson, B. J., Wyllie, A. H. & Rich, T. New insights into the role of PML in tumour suppression. *Cell Res* **18**, 622-40 (2008).
5. Ishov, A. M. et al. PML is critical for ND10 formation and recruits the PML-interacting protein daxx to this nuclear structure when modified by SUMO-1. *J Cell Biol* **147**, 221-34 (1999).
6. Jensen, K., Shiels, C. & Freemont, P. S. PML protein isoforms and the RBCC/TRIM motif. *Oncogene* **20**, 7223-33 (2001).
7. Bernardi, R. & Pandolfi, P. P. Structure, dynamics and functions of promyelocytic leukaemia nuclear bodies. *Nat Rev Mol Cell Biol* **8**, 1006-16 (2007).
8. Bischof, O. et al. Deconstructing PML-induced premature senescence. *Embo J* **21**, 3358-69 (2002).
9. Ferbeyre, G. et al. PML is induced by oncogenic ras and promotes premature senescence. *Genes Dev* **14**, 2015-27 (2000).
10. Pearson, M. et al. PML regulates p53 acetylation and premature senescence induced by oncogenic Ras. *Nature* **406**, 207-10 (2000).
11. Gurrieri, C. et al. Loss of the tumor suppressor PML in human cancers of multiple histologic origins. *J Natl Cancer Inst* **96**, 269-79 (2004).
12. Scaglioni, P. P. et al. A CK2-dependent mechanism for degradation of the PML tumor suppressor. *Cell* **126**, 269-83 (2006).

13. Trotman, L. C. et al. Identification of a tumour suppressor network opposing nuclear Akt function. *Nature* **441**, 523-7 (2006).
14. Dehay, C. & Kennedy, H. Cell-cycle control and cortical development. Nat *Rev Neurosci* **8**, 438-50 (2007).
15. Caviness, V. S., Jr. et al. Cell output, cell cycle duration and neuronal specification: a model of integrated mechanisms of the neocortical proliferative process. *Cereb Cortex* **13**, 592-8 (2003).
16. Frederiksen, K. & McKay, R. D. Proliferation and differentiation of rat neuroepithelial precursor cells in vivo. *J Neurosci* **8**, 1144-51 (1988).
17. Haubensak, W., Attardo, A., Denk, W. & Huttner, W. B. Neurons arise in the basal neuroepithelium of the early mammalian telencephalon: a major site of neurogenesis. *Proc Natl Acad Sci U S A* **101**, 3196-201 (2004).
18. Hevner, R. F. From radial glia to pyramidal-projection neuron: transcription factor cascades in cerebral cortex development. *Mol Neurobiol* **33**, 33-50 (2006).
19. Tropepe, V. et al. Distinct neural stem cells proliferate in response to EGF and FGF in the developing mouse telencephalon. *Dev Biol* **208**, 166-88 (1999).
20. Alcalay, M. et al. The promyelocytic leukemia gene product (PML) forms stable complexes with the retinoblastoma protein. *Mol Cell Biol* **18**, 1084-93 (1998).
21. Labbaye, C. et al. Expression and role of PML gene in normal adult hematopoiesis: functional interaction between PML and Rb proteins in erythropoiesis. *Oncogene* **18**, 3529-40 (1999).
22. Mallette, F. A., Goumard, S., Gaumont-Leclerc, M. F., Moiseeva, O. & Ferbeyre, G. Human fibroblasts require the Rb family of tumor suppressors, but not p53, for PML-induced senescence. *Oncogene* **23**, 91-9 (2004).
23. Jacks, T. et al. Effects of an Rb mutation in the mouse. *Nature* **359**, 295-300 (1992).
24. Lipinski, M. et al. Comparison of exercise test scores and physician estimation in determining disease probability. *Arch Intern Med* **161**, 2239-44 (2001).
25. Ferguson, K. L. et al. Telencephalon-specific Rb knockouts reveal enhanced neurogenesis, survival and abnormal cortical development. *Embo J* **21**, 3337-46 (2002).
26. Marino, S., Hoogervoorst, D., Brandner, S. & Berns, A. Rb and p107 are required for normal cerebellar development and granule cell survival but not for Purkinje cell persistence. *Development* **130**, 3359-68 (2003).
27. MacPherson, D. et al. Cell type-specific effects of Rb deletion in the murine retina. *Genes Dev* **18**, 1681-94 (2004).
28. Ferguson, K. L. et al. A cell-autonomous requirement for the cell cycle regulatory protein, Rb, in neuronal migration. *Embo J* **24**, 4381-91 (2005).
29. Sherr, C. J. Cancer cell cycles. *Science* **274**, 1672-7 (1996).
30. Alberts, A. S., Thorburn, A. M., Shenolikar, S., Mumby, M. C. & Feramisco, J. R. Regulation of cell cycle progression and nuclear affinity of the retinoblastoma protein by protein phosphatases. *Proc Natl Acad Sci U S A* **90**, 388-92 (1993).
31. Durfee, T. et al. The retinoblastoma protein associates with the protein phosphatase type 1 catalytic subunit. *Genes Dev* **7**, 555-69 (1993).
32. Kim, T. H., Goodman, J., Anderson, K. V. & Niswander, L. Phactr4 regulates neural tube and optic fissure closure by controlling PP1-, Rb-, and E2F1-regulated cell-cycle progression. *Dev Cell* **13**, 87-102 (2007).

33. de Bruin, A. et al. Rb function in extraembryonic lineages suppresses apoptosis in the CNS of Rb-deficient mice. *Proc Natl Acad Sci U S A* **100**, 6546-51 (2003).
34. Shen, Q. et al. The timing of cortical neurogenesis is encoded within lineages of individual progenitor cells. *Nat Neurosci* **9**, 743-51 (2006).
35. Bellodi, C. et al. Cytoplasmic function of mutant promyelocytic leukemia (PML) and PML-retinoic acid receptor-alpha. *J Biol Chem* **281**, 14465-73 (2006).

FIGURES LEGENDS

Figure 1 Pml expression is confined to neural progenitor cells
(**a**) Expression of Pml in coronal section of *Pml+/-* E15 embryo neocortex. Sections were also stained for Nestin, which is a marker of progenitors in the ventricular zone (VZ), and Map2, which is a marker of mature neurons in the cortical plate (CP). Pml expression encompasses the Nestin progenitor domain but is absent in the Map2+ domain. Close-up images show Pml accumulation in nuclei of neural progenitor cells (NPC, top right panel). Bottom left panel shows anti-Pml staining in the *Pml-/-* cortex. Scale bars: 200μm and 10μm. (**b**) βIIITubulin (βIIITub)+ cells are negative for Pml expression in the VZ and CP. Coronal section of *Pml+/-* E15 embryo cerebral cortex were stained with anti-βIIITub and anti-Pml antibodies. Arrowheads indicate βIIITub+ cells in the VZ. (**c**) Expression of Pml in coronal section of *Pml+/-* cerebral cortex at P0 was performed as in Fig. 1. (**d**) Expression of Pml at the level of the lateral ventricles at P7. Scale bars: 200 μm. For both c and d, haematoxylin and eosin (H&E)-stained coronal sections stained shown to highlight areas on which the immunohistochemical analysis was performed (boxed).

Figure 2 Pml regulates the size of the cerebral cortex.
(**a**) Images of *Pml-/-* brains (n=12 mice) show a clear reduction in size when compared to *Pml +/+* (n=5 mice) and *Pml+/-* (n=15 mice). Graphs show width and length of cortices from P0 *Pml-/-*, *Pml +/+* and *Pml +/-* animals. Graphs show mean ± s.e.m. of cortex width and length ($p < 0.0001$, unpaired t-test, two tails; also for the following figures, unless stated otherwise). (**b**) Coronal sections stained with haematoxylin and eosin (H&E) indicate smaller brain size in the *Pml -/-* compared to *Pml+/-* animals at P0. (**c**) Thickness of the cortex wall is reduced in Pml-deficient P0 brains. Coronal sections of Pml+/- and Pml-/- P0 brains were stained with H&E and the cortex thickness was measured (Axiovert, Germany). Histogram shows mean ± s.e.m. of cortex thickness (**p=0.00025). (**d**) Coronal sections through *Pml+/-* and *Pml-/-* adult brains were stained with H&E and analysed using Axiovert for cortex wall thickness. A to E indicate areas (500 μm) of brain sectioning, while numbers indicate sections (10 μm) for each area. Hippocampus is present in sections starting at D2. Graph shows means ± s.e.m (n=3 each genotype; B3 *p=0.0273; C1 *p=0.0384; C2 *p=0.0154; C3 *p=0.0296; D1 *p=0.010; D2 *p=0.0493). **b**, Representative images of section B3. Scale bar: 200 μm. Striatum is indicated (S).

Figure 3: Pml controls proliferation and the cell cycle exit in neuronal progenitors.
(**a**) Increased number of Ki67+ cells in *Pml-/-* E15 embryos. Immunohistochemistry with anti-Ki67 proliferation marker on coronal sections through the cerebral cortex of E15 *Pml+/-* and *Pml-/-* embryos. (**b**) Increased number of mitotic cells at the apical surface of *Pml-/-* E15 embryos. Immunohistochemistry with anti-phosphorylated histone H3 (P-H3) and βIIITub antibodies on coronal sections through the cerebral cortex of E15 *Pml+/-* and *Pml-/-* embryos. Histogram shows mean ± s.e.m. of number of P-H3+ cells (**p=0.0077). (**c**) Increased number of cells in S-phase in Pml-deficient ventricular zone (VZ). Anti-BrdU-fluorescin isothiocyanate (FITC; green) on coronal sections through the cerebral cortex of E15 *Pml+/-* and *Pml-/-* embryos isolated from pregnant mice after a one hour BrdU pulse. Histogram shows mean ± stdev of BrdU+ cells in images of 3 different stained sections from 3 different embryos for each genotype (n=3 *Pml-/-* compared to n=3 *Pml +/-* littermates control;

*p = 0.0317). (**d**) Immunohistochemistry with anti-BrdU-FITC and anti-Ki67 on coronal sections through the cerebral cortex of E15 *Pml+/-* and *Pml-/-* embryos obtained from pregnant mice injected with BrdU for 24 hours. The number of BrdU+/Ki67- (cells that exited cell cycle) and BrdU+/Ki67+ (cells in cycle) present in the *Pml-/-* VZ and cortical plate was analyzed. The graph expresses the mean ± stdev of the number of BrdU+/Ki67+ in *Pml-/-* versus *Pml+/-* intermediate zone in two images of two different stained sections from two different embryos for each genotype (n=2 *Pml-/-* compared to n=2 *Pml +/-* littermates controls; *p = 0.0196). Scale bar: 20μm in.

Figure 4 Pml loss skews the composition of neural progenitors subtypes in the developing neocortex, (**a**) Increased number of radial glial cells in Pml-deficient cortices. Immunohistochemistry with anti-Pax6 and βIIITub antibodies through the cerebral cortex of E15 *Pml+/-* (top) and *Pml-/-* (bottom) embryos. (**b**) Reduction in basal progenitors in *Pml-/-* cortices. Brains were stained with an antibody against Tbr2, a marker of basal progenitors. (**c**) reduction basally located mitoses (P-H3+) in Pml-deficient brains. Histogram shows mean ± s.e.m of P-H3+ cells numbers (11 separate sections each genotype; *p=0.0178).

Figure 5 The overall number of neurons is reduced in *Pml*-/- cortices, while cortical architecture is not affected
(**a**) Immunohistochemistry with the neuronal marker Map2 on E15 *Pml+/-* and *Pml-/-* coronal sections through the cerebral cortex shows a reduced size of the cortical plate in *Pml-/-* embryos compared to *Pml+/-* (Left panel). Less Map2+ (neurons) were generated in the *Pml-/-* cerebral cortex compared to the *Pml+/-* (right panel). Scale bar: 200μm. (**b**) Immunohistochemistry with the neuronal marker Map2 on P0 *Pml+/-* and *Pml-/-* coronal sections through the cerebral cortex shows a reduced size of the cortical plate in *Pml-/-* embryos compared to the *Pml+/-* (Left panel). Scale bar: 200μm. The number of MAP2+ cells was determined by counting Dapi+/MAP2+ cells in two images of two different sections for each genotype (n=2 *Pml-/-* and n=2 *Pml +/-* littermates; a **p = 0.002, b **p = 0.0028). (**c, d**) The overall architecture of the cortex is maintained in Pml-deficient brains. Immunohistochemistry with anti-Foxp1 (**c**) and anti-Foxp2 (**d**) on coronal sections through the cerebral cortex from *Pml+/-* (upper panels) and *Pml-/-* (lower panels) pups at P0. While Foxp1+ neurons are found in layers 3,4,5, Foxp2 specifies layer neurons. The graphs show the number of Foxp1+ and Foxp2+ cells from two similarly sized images from 2 different stained sections for each genotype (n=2 *Pml-/-* compared to n=2 *Pml +/-* littermates control). Scale bars: 200μm (c) and 100μm (d). *p = 0.0162 (c), *p = 0.0294 (d).

Figure 6 *Pml*-deficient NPCs display increased proliferation and impaired differentiation *in vitro*
(**a**) Pml loss causes increased proliferation in neurospheres cultures derived from E12 NPCs. Representative image showing the size of *Pml-/-* primary neurospheres compared to *Pml*+/-. Histogram shows mean ± stdev of neurosphere diameter, which measured in 10 live images / genotype (n=2 Pml+/- and n=2 Pml +/- littermates; **p=0.0056). (**b**) Differentiation is impaired in *Pml-/-* cultures. Neurosphere differentiation assays using cortical progenitors from *Pml+/-* (upper set of panels) and *Pml-/-* embryos at E12 (lower set of panels). The number of Nestin+ (precursors), Map2+ (neurons), GFAP+ (astrocytes) and MBP+ (oligodendrocytes) were counted. The percentage of Nestin versus differentiated cells (Map2+, GFAP+ or MBP+) was

determined in two immunoflurescence images for each embryo (n=3 *Pml-/-* and n=3 *Pml +/-* littermate embryos; left panel: **p = 0.0018 and *p = 0.0351; middle panel: **p = 0.0015 and **p = 0.0085; right panel: *p = 0.0256 and **p = 0.0015. (**d, e**) Reintroduction of PML I, but not of PMLI ΔSUMO reduces proliferation and rescues differentiation *in vitro*. NPCs were infected with PML I or PMLI ΔSUMO pBabe viruses and assayed for their proliferation and differentiation capacity. (**d**) Neurosphere proliferation assays were performed as described above. The diameter of neurospheres was determined in 16 live images/sample in culture of uninfected or infected cells; representative of two independent experiments. (**e**) PML I, but not PMLI ΔSUMO promotes differentiation of progenitors *in vitro*. Neurosphere differentiation assay were performed as in (a). Representative of two independent experiments.

Figure 7 Pml interacts and colocalises with pRb

(**a**) Immunohistochemistry with anti-Pml and anti-pRb antibodies on coronal sections from E15 *Pml+/-* (first and third set of panels from top) and *Pml-/-* (second and fourth set of panels) embryos (40X; scale bar: 50 μm). High magnification images of the VZ (third and fourth set of panels) show pRb and Pml colocalization (63X). The last set of panels shows that pRb accumulates in both the nucleus and the cytoplasm in the *Pml-/-* VZ. Arrowhead indicates cells in the *Pml-/-* cortical plate displaying nuclear pRb staining. Scale bars: 5μm (lower two set of panels). (**b**) pRb is found in immunoprecipitates from *Pml+/-* but not *Pml-/-* extracts. Immunoprecipitation with an anti-Pml antibody from *Pml+/-* and *Pml-/-* extracts. Input lanes show pRb and Pml expression in *Pml+/-* and *Pml-/-* NPCs. β-actin was measured as loading control.

Figure 8 Pml-mediated control of PP1α-dependent dephosphorylation of pRb in the NPCs

(a) pRb is hyperphosphorylated in Pml-deficient NPCs. Immunoblotting of extracts from *Pml+/-* and *Pml-/-* NPCs using an anti-pRb antibody shows an increase in the level of the pRb hyper-phosphorylated form (*) in *Pml-/-* extracts. The expression of Pml was analysed using an anti-Pml antibody. Anti-β-actin antibody was used as loading control. (**b**) PP1α localisation is altered in *Pml-/-* cortices. Immunohistochemistry with anti-Pml (red), anti-pRb (green) and anti-PP1α (purple) antibodies was performed on coronal sections from *Pml+/-* E15 embryos (ventricular zone). (**c**) PML partially colocalises with pRb and PP1a in vivo, and PP1α localisation is altered in Pml-deficient cortices. Sections were stained as in (b) (scale bars: 5 μm). (**d**) Immunofluorescence of control (+/-) and *Pml-/-* cortical NPCs stained with anti-Pml (red), -pRb (green) and -PP1α (purple) antibodies. DAPI was used for nuclear staining. Scale bars: 5μm. (**e**) Both PP1α and pRb are found in anti-Pml immunoprecipitates. Immunoprecipitation of Pml was performed as in Fig. 7c using extracts from *Pml+/-* and *Pml-/-* NPCs. Immunoprecipitates were run on a 10% SDS-PAGE and probed with an anti-pRb, Pml and PP1α antibody (upper panel). Inputs show pRb, Pml and PP1α expression. (**f**) PML I, but not PMLI ΔSUMO, expression in Pml-deficient NPCs reduces pRb phosphoryation. Hyper- and hypo-phosphorylated forms of pRb were analyzed using an anti-pRb antibody in extracts from *Pml-/-* progenitors uninfected or infected with pBabe pBabe-PMLI and pBabe-PMLI ΔSUMO viruses. Pml and PP1α were also detected using specific antibodies. β-actin was measured as loading control.

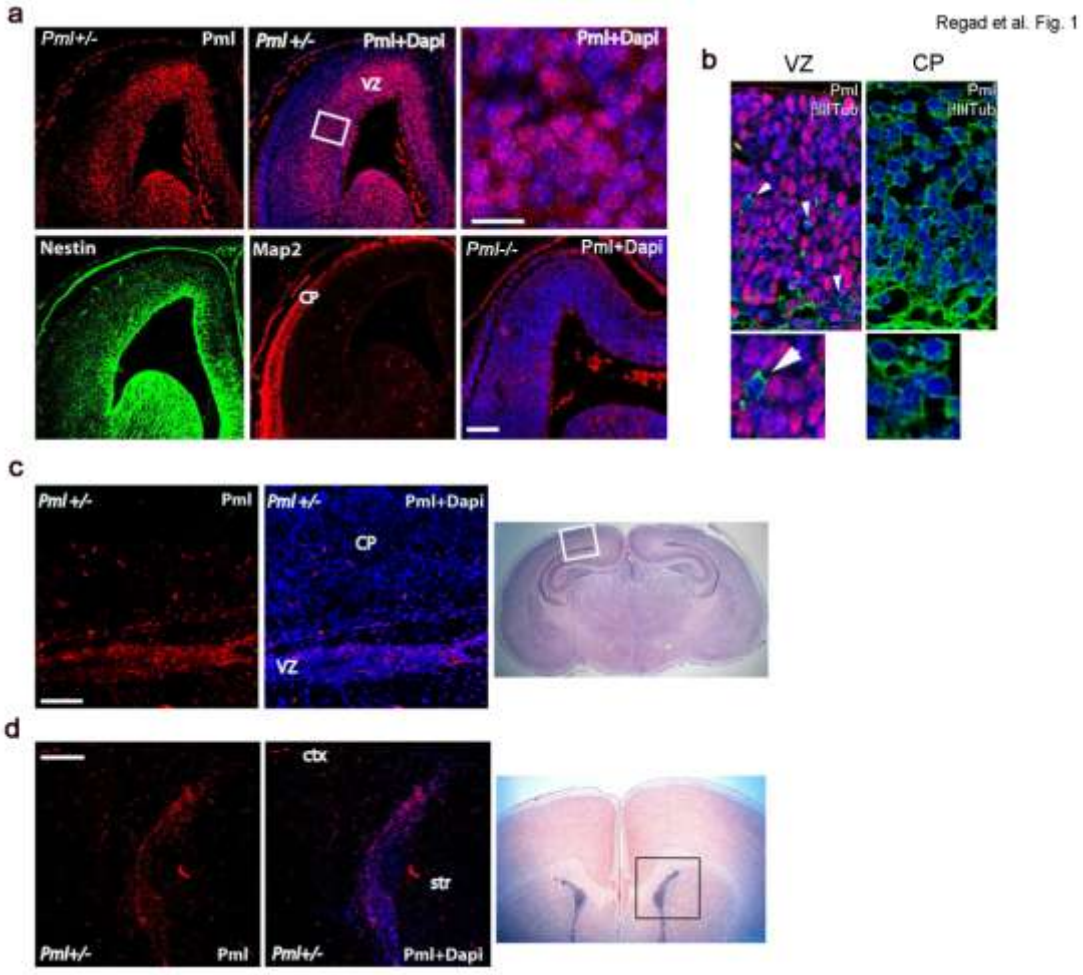

Regad et al. Fig. 1

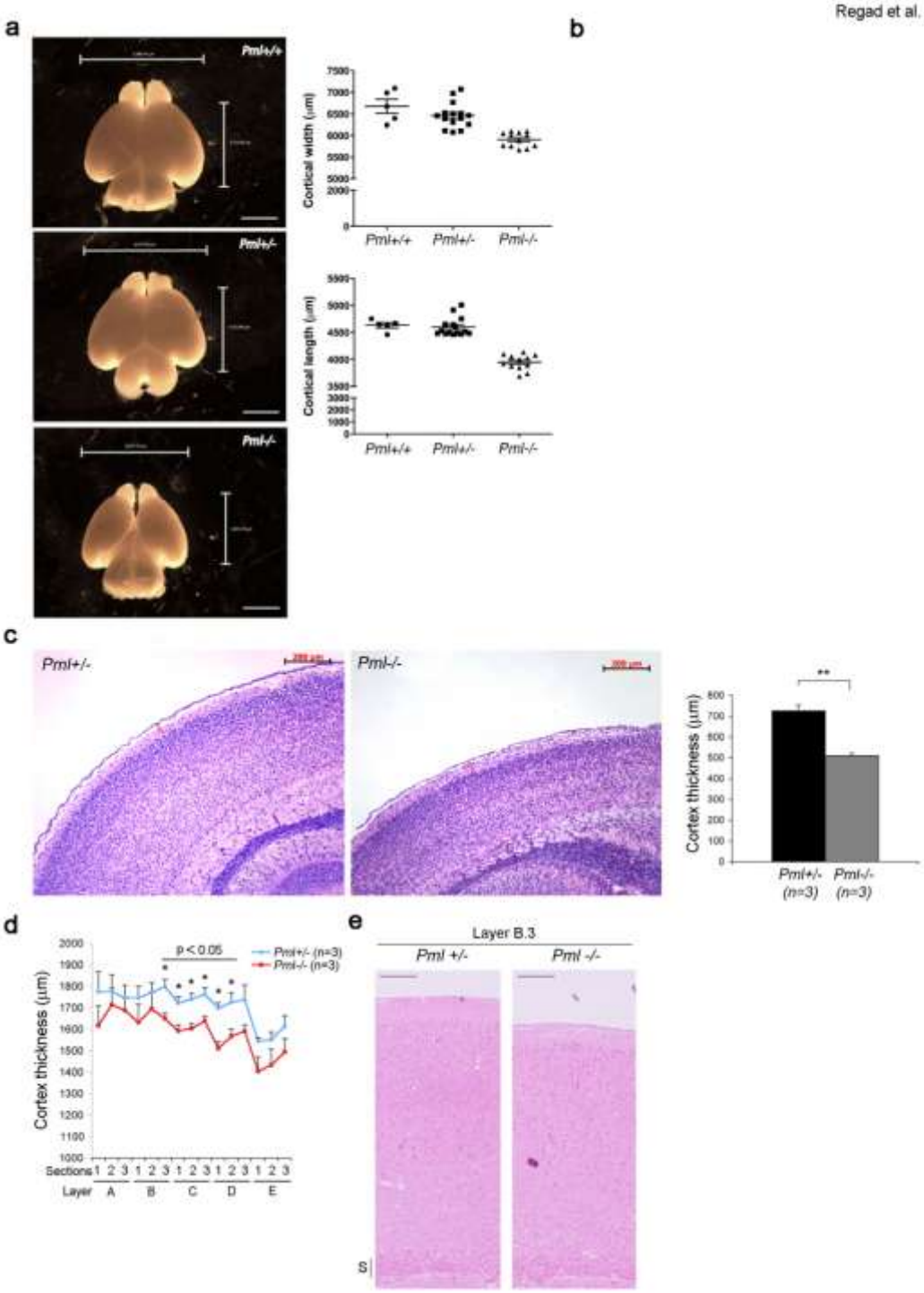
a
Pml+/+
Pml+/-
Pml-/-
b
Cortical width (µm)
Cortical length (µm)
Pml+/+
Pml+/-
Pml-/-
c
Pml+/-
Pml-/-
Cortex thickness (µm)
**
Pml+/- (n=3)
Pml-/- (n=3)
d
Cortex thickness (µm)
p < 0.05
Pml+/- (n=3)
Pml-/- (n=3)
Sections
Layer
A
B
C
D
E
e
Layer B.3
Pml +/-
Pml -/-
S

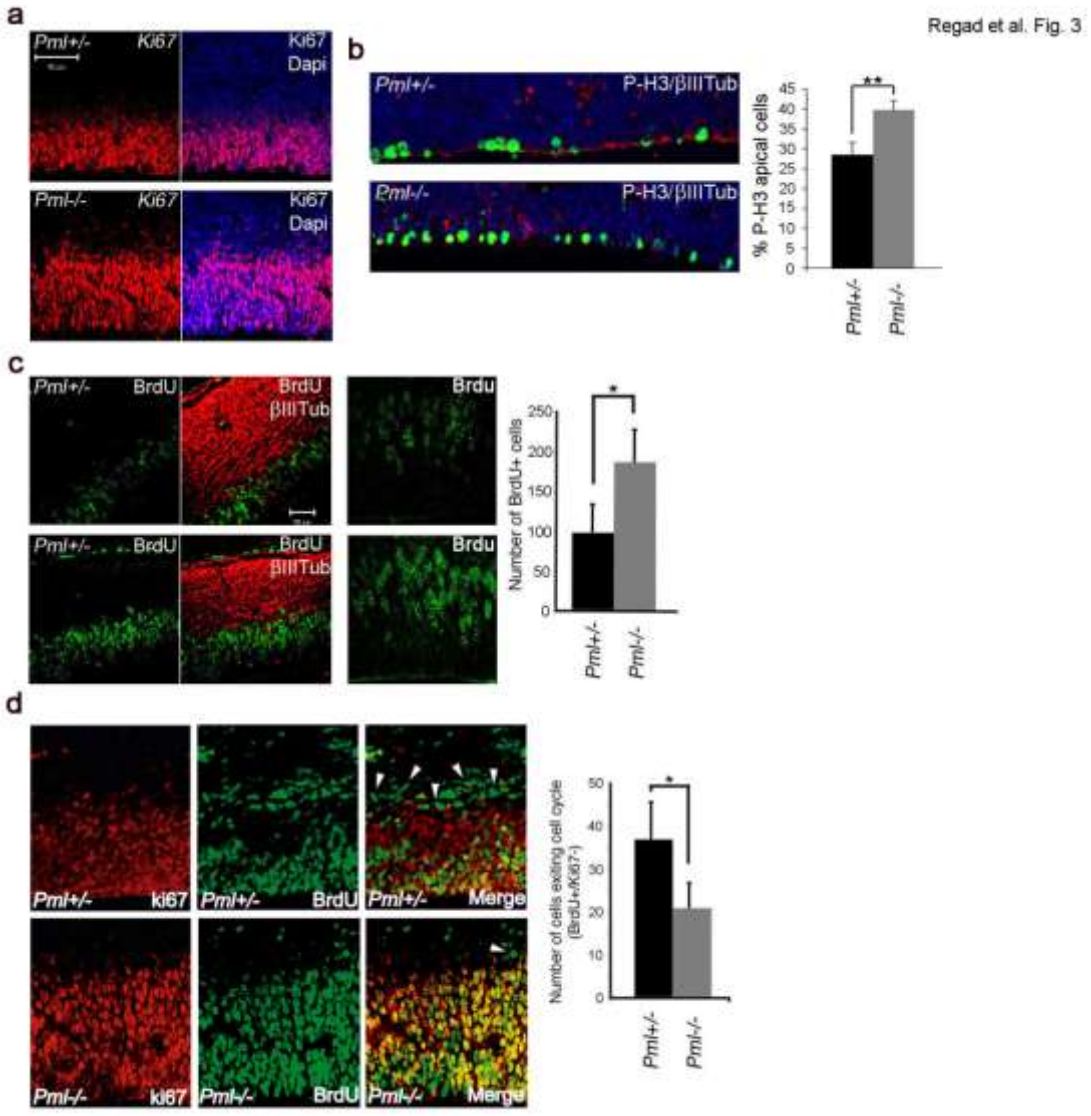

Regad et al. Fig. 3

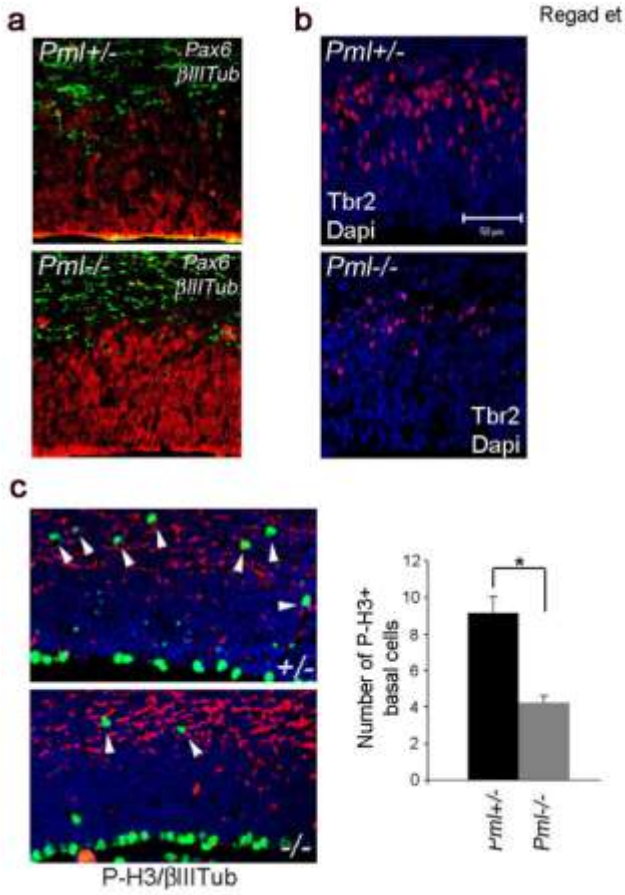
Regad et al. Fig. 4
a
Pml+/-
Pax6
βIIITub
Pml-/-
Pax6
βIIITub
b
Pml+/-
Tbr2
Dapi
Pml-/-
Tbr2
Dapi
c
+/-
-/-
P-H3/βIIITub
Number of P-H3+ basal cells
12
10
8
6
4
2
0
*
Pml+/-
Pml-/-

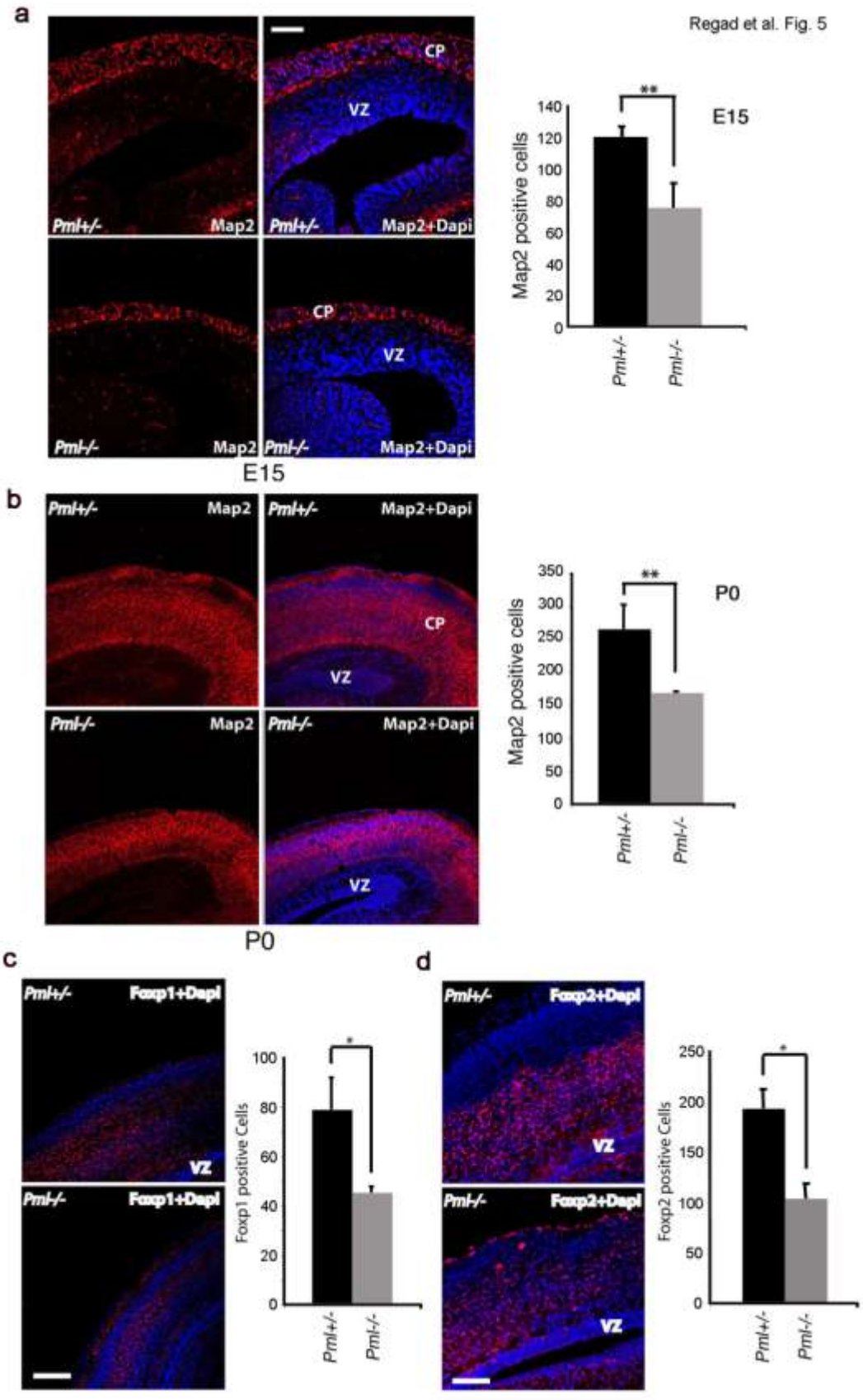
Regad et al. Fig. 5
a
Pml+/-
Map2
Pml+/-
Map2+Dapi
CP
VZ
Pml-/-
Map2
Pml-/-
Map2+Dapi
CP
VZ
E15
Map2 positive cells
140
120
100
80
60
40
20
0
**
E15
Pml+/-
Pml-/-
b
Pml+/-
Map2
Pml+/-
Map2+Dapi
CP
VZ
Pml-/-
Map2
Pml-/-
Map2+Dapi
VZ
P0
Map2 positive cells
350
300
250
200
150
100
50
0
**
P0
Pml+/-
Pml-/-
c
Pml+/-
Foxp1+Dapi
VZ
Pml-/-
Foxp1+Dapi
Foxp1 positive Cells
100
80
60
40
20
0
*
Pml+/-
Pml-/-
d
Pml+/-
Foxp2+Dapi
VZ
Pml-/-
Foxp2+Dapi
VZ
Foxp2 positive Cells
250
200
150
100
50
0
*
Pml+/-
Pml-/-

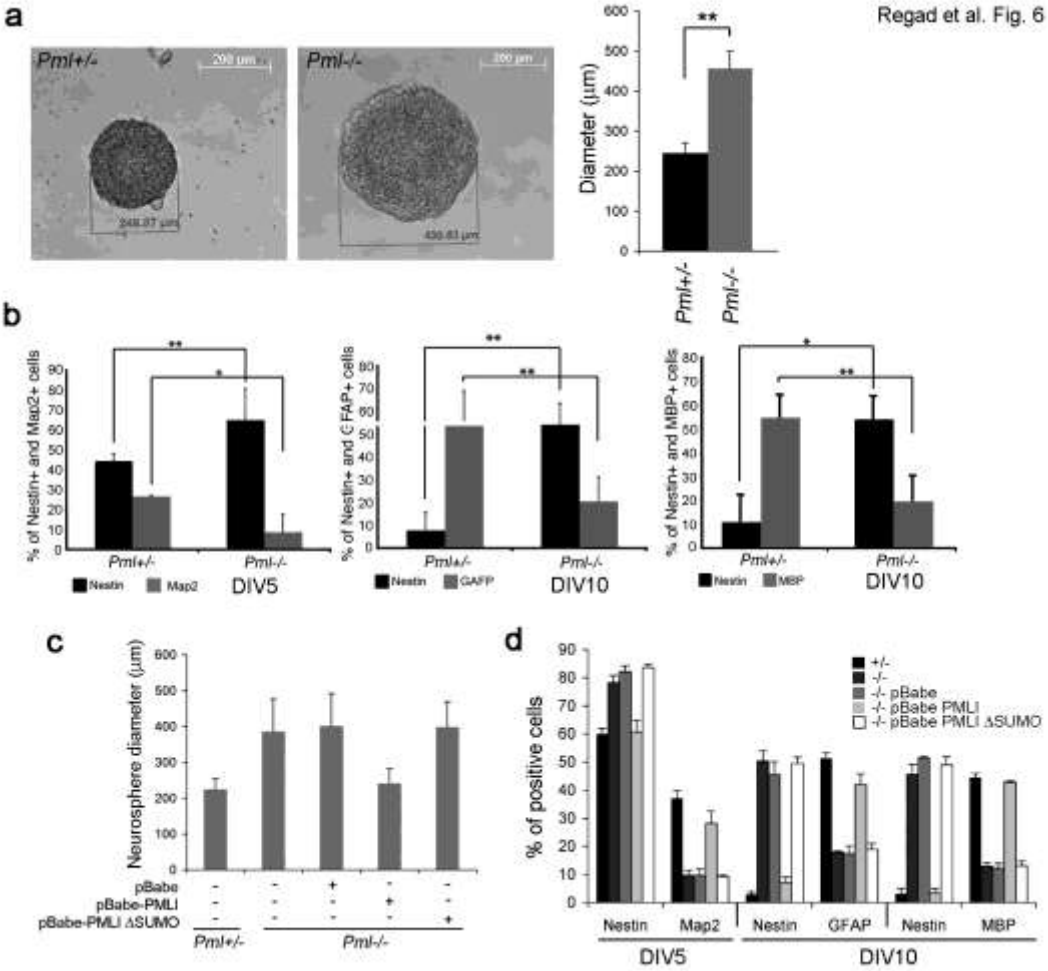
Regad et al. Fig. 6
a
Pml+/-
Pml-/-
Diameter (µm)
b
% of Nestin+ and Map2+ cells
% of Nestin+ and GFAP+ cells
% of Nestin+ and MBP+ cells
Nestin
Map2
GAFP
MBP
DIV5
DIV10
c
Neurosphere diameter (µm)
pBabe
pBabe-PMLI
pBabe-PMLI ΔSUMO
d
% of positive cells
+/-
-/-
-/- pBabe
-/- pBabe PMLI
-/- pBabe PMLI ΔSUMO
Nestin
Map2
GFAP
MBP

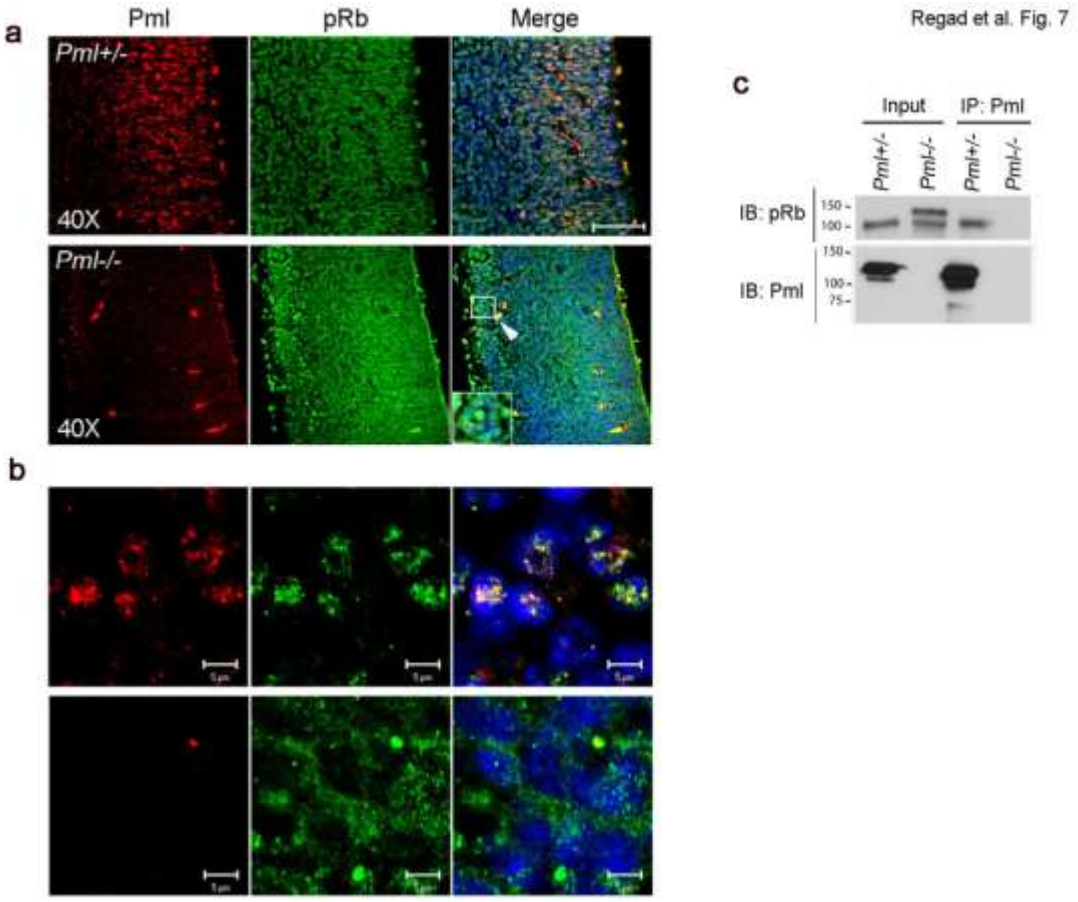
Regad et al. Fig. 7
a
Pml
pRb
Merge
Pml+/-
40X
Pml-/-
40X
b
c
Input
IP: Pml
Pml+/-
Pml-/-
Pml+/-
Pml-/-
IB: pRb
150
100
IB: Pml
150
100
75

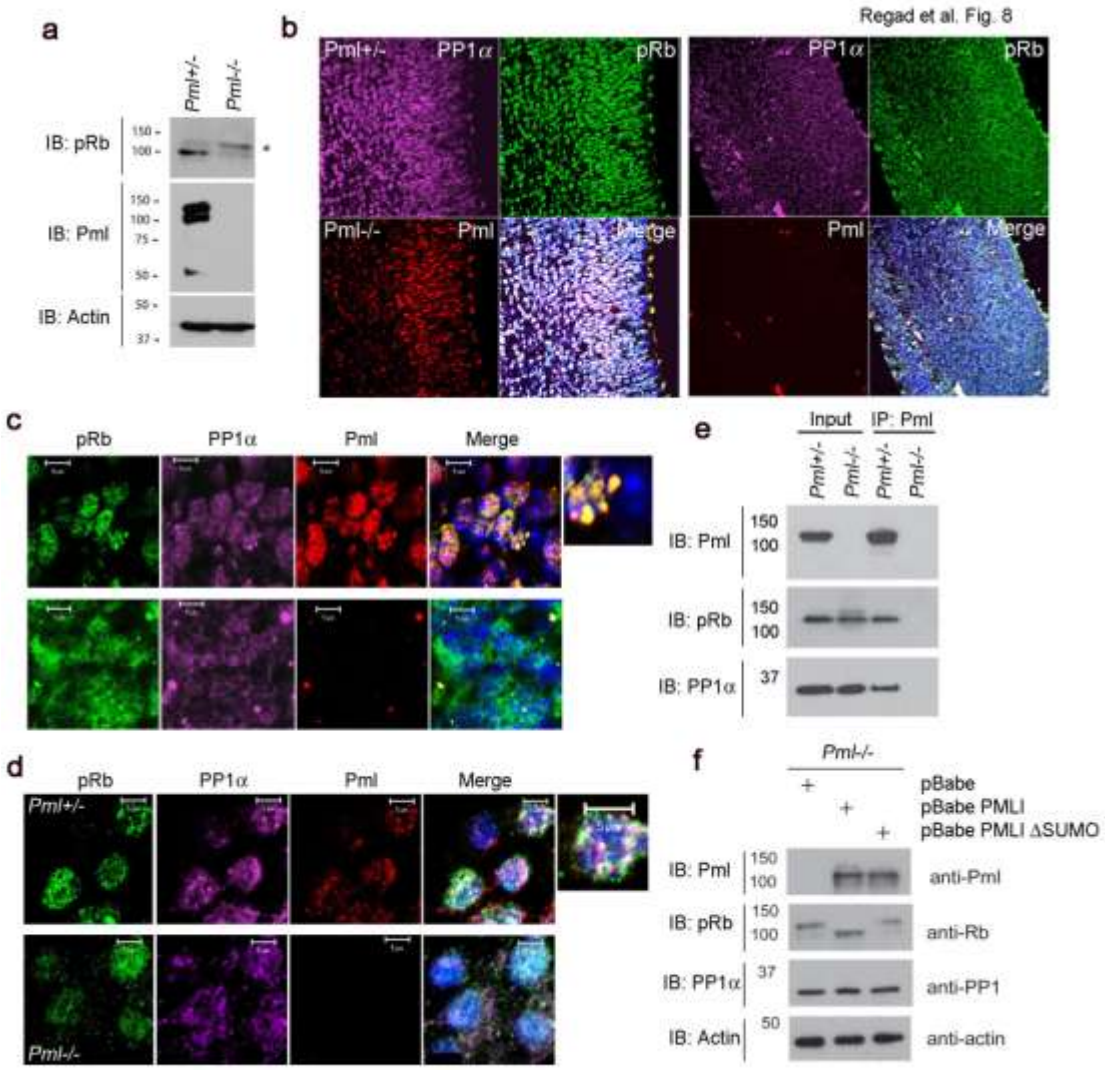
Regad et al. Fig. 8
a
Pml+/-
Pml-/-
IB: pRb
IB: Pml
IB: Actin
b
Pml+/-
PP1α
pRb
Pml-/-
Pml
Merge
c
pRb
PP1α
Pml
Merge
d
Pml+/-
Pml-/-
e
Input
IP: Pml
IB: Pml
IB: pRb
IB: PP1α
f
Pml-/-
pBabe
pBabe PMLI
pBabe PMLI ΔSUMO
IB: Pml
IB: pRb
IB: PP1α
IB: Actin
anti-Pml
anti-Rb
anti-PP1
anti-actin